



1 **Large contribution of soil emissions to the atmospheric nitrogen**
2 **budget and their impacts on air quality and temperature rise in**
3 **North China**

4 *Tong Sha^{1*}, Siyu Yang¹, Qingcai Chen¹, Liangqing Li¹, Xiaoyan Ma², Yan-Lin Zhang^{3,4},*
5 *Zhaozhong Feng³, K. Folkert Boersma^{5,6}, Jun Wang^{7*}*

6 ¹ School of Environmental Science and Engineering, Shaanxi University of Science and
7 Technology, Xi'an 710021, China

8 ² Key Laboratory for Aerosol-Cloud-Precipitation of China Meteorological
9 Administration, Nanjing University of Information Science & Technology, Nanjing
10 210044, China

11 ³ School of Ecology and Applied Meteorology, Nanjing University of Information
12 Science & Technology, Nanjing 210044, China

13 ⁴ Atmospheric Environment Center, Joint Laboratory for International Cooperation on
14 Climate and Environmental Change, Ministry of Education (ILCEC), Nanjing
15 University of Information Science & Technology, Nanjing 210044, China

16 ⁵ Satellite Observations Department, Royal Netherlands Meteorological Institute, De
17 Bilt 3731GA, the Netherlands

18 ⁶ Meteorology and Air Quality Group, Wageningen University Wageningen 6708PB,
19 the Netherlands

20 ⁷ Department of Chemical and Biochemical Engineering, Center for Global and
21 Regional Environmental Research, and Iowa Technology Institute, University of Iowa,
22 Iowa City, IA, 52242, USA



23 *Corresponding authors:

24 Tong Sha: tong-sha@sust.edu.cn

25 Jun Wang, jun-wang-1@uiowa.edu

26



27 **Abstract**

28 Soil emissions of nitrogen compounds, including NO and HONO, play a
29 significant role in atmospheric nitrogen budget. However, HONO has been overlooked
30 in previous research on soil reactive nitrogen (Nr) emissions and their impacts on air
31 quality in China. This study estimates both soil NO_x and HONO emissions (SNO_x and
32 SHONO) in North China with an updated soil Nr emissions scheme in a chemical
33 transport model, the Unified Inputs for WRF-Chem (UI-WRF-Chem). The effects of
34 soil Nr emissions on O₃ pollution, air quality and temperature rise are also studied, with
35 a focus on two key regions, Beijing-Tianjin-Hebei (BTH) and Fenwei Plain (FWP),
36 known for high soil Nr and anthropogenic emissions. We find that the flux of SNO_x is
37 nearly doubled those of SHONO; the monthly contributions of SNO_x and SHONO
38 account for 37.3% and 13.5% of anthropogenic NO_x emissions in the BTH, and 29.2%
39 and 19.2% in the FWP during July 2018, respectively. Soil Nr emissions have a
40 significant impact on surface O₃ and nitrate, exceeding SNO_x or SHONO effects alone.
41 On average, soil Nr emissions increase MDA8 O₃ by 16.9% and nitrate concentrations
42 by 42.4% in the BTH, 17.2% for MDA8 O₃ and 42.7% for nitrate in the FWP. Reducing
43 anthropogenic NO_x emissions leads to a more substantial suppressive effect of soil Nr
44 emissions on O₃ mitigation, particularly in BTH. Soil Nr emissions, via their role as
45 precursors for secondary inorganic aerosols, can result in a slower increase rate of
46 surface air temperature. This study suggests that mitigating O₃ pollution and addressing
47 climate change in China should consider the role of soil Nr emission, and their regional
48 differences.



49 **1. Introduction**

50 Surface ozone (O_3) is a major air pollutant harmful to human health, terrestrial
51 vegetation, and crop growth (Feng et al., 2022b; Turner et al., 2016; Unger et al., 2020;
52 Yue et al., 2017). China is confronting serious O_3 pollution, with the surface O_3
53 concentrations routinely exceeding air quality standards (Li et al., 2019). Although the
54 Chinese Action Plan on Air Pollution Prevention and Control implemented in 2013 has
55 significantly reduced the nationwide anthropogenic emissions of primary pollutants
56 including particulate matter (PM) and nitrogen oxides ($NO_x = NO + NO_2$), the
57 summertime O_3 concentrations observed by national ground sites and satellite
58 observations both show an increasing trend of 1-3 ppbv a^{-1} in megacity clusters of
59 eastern China from 2013 to 2019 (Wang et al., 2022b; Wei et al., 2022). Many studies
60 have explored the causes of O_3 pollution from the perspective of changes in
61 meteorology and anthropogenic emissions, and attributed the O_3 increase to decreased
62 PM levels and anthropogenic NO_x emissions, and adverse meteorological conditions
63 (Li et al., 2021b; Li et al., 2019; Li et al., 2020; Liu and Wang, 2020a, b; Lu et al., 2019).

64 Soil emissions are an important natural source of reactive nitrogen species,
65 including N_2O , NO_x , HONO and NH_3 , and can strongly affect the atmospheric
66 chemistry, air pollution and climate change (Elshorbany et al., 2012; Pinder et al., 2012).
67 It has been acknowledged that the soils emissions account for 12-20% of total emissions
68 of NO_x in global average (Vinken et al., 2014; Yan et al., 2005), and 40-51% in
69 agricultural regions during periods in which fertilizers are applied to soils, resulting in
70 a significant increase in O_3 and NO_2 concentrations in US (Almaraz, 2018; Romer et



71 al., 2018; Sha et al., 2021; Wang et al., 2021a), Europe (Skiba et al., 2020) and sub-
72 Saharan Africa (Huang et al., 2018).

73 China has a large area of cultivated land ($\sim 1.276 \times 10^6$ km²,
74 http://gi.mnr.gov.cn/202304/t20230414_2781724.html, last access: 18th December
75 2023), which contributes to one-third of the global nitrogen fertilizer use and has
76 extensive nitrogen deposition (Liu et al., 2013; Lu and Tian, 2017; Reay, 2008). So far,
77 only a limited studies focused on the impact of soil NO_x emissions (denoted as SNO_x)
78 on O₃ pollution in China (Huang et al., 2023; Lu et al., 2021; Shen et al., 2023; Wang
79 et al., 2008; Wang et al., 2023a; Wang et al., 2022a). Lu et al. (2021) demonstrated that
80 the presence of SNO_x in the North China Plain significantly reduced the sensitivity of
81 surface O₃ to anthropogenic emissions. Huang et al. (2023) suggested that substantial
82 SNO_x could increase the maximum daily 8 h (MDA8) O₃ concentrations by 8.0–12.5
83 $\mu\text{g m}^{-3}$ on average for June 2018 in China. These studies focused only on NO_x emitted
84 from soils, and neglected that similar soil microbial activities also emit nitrous acid
85 (HONO). The measurements in laboratory showed that the emission rates of soil HONO
86 were comparable to those of NO (Oswald et al., 2013; Weber B, 2015). The photolysis
87 of HONO has been identified to be an important source of atmospheric hydroxyl radical
88 ($\cdot\text{OH}$), which enhances concentrations of hydroperoxyl (HO₂) and organic peroxy
89 radicals (RO₂), accelerating the conversion of NO to NO₂, resulting in more
90 concentrations of O₃ and secondary pollutants. Although the sources and formation
91 mechanisms of HONO are still not fully understood, recent model studies suggested
92 that HONO emission from soils in the agriculture-intensive North China Plain could



93 increase the regionally averaged daytime $\cdot\text{OH}$, O_3 , and daily fine particulate nitrate
94 concentrations (Feng et al., 2022a; Wang et al., 2021b).

95 Only a few studies simultaneously considered the impact of soil HONO emissions
96 (denoted as SHONO) along with SNO_x on O_3 and other secondary pollutants (Tan et
97 al., 2023; Wang et al., 2023b). Wang et al. (2023b) found that the NO_x and HONO
98 emissions from natural soils (i.e., soil background emissions) increased daily average
99 O_3 concentrations by 2.0% in Northeast Plain during August 2016 without considering
100 the contribution from fertilized croplands. Tan et al. (2023) believed that the
101 contribution of soil NO_x and HONO to O_3 pollution has been in an increasing trend
102 from 2013 (5.0 pptv) to 2019 (8.0 pptv) in the summer season over the North China
103 Plain by using the GEOS-Chem model; however the coarse resolution of GEOS-Chem
104 simulation may not insufficient to resolve the spatial heterogeneity in soil emission
105 distribution (Lu et al., 2021). Associated with the decreasing anthropogenic emissions
106 is the increasing contribution of soil emissions to the atmospheric nitrogen budget in
107 China. Therefore, it is critical to quantify the impact of soil reactive nitrogen (Nr: NO_x
108 and HONO) emissions on O_3 and secondary pollutants.

109 In this study, we improve the soil Nr emissions scheme in the Unified Inputs
110 (initial and boundary conditions) for Weather Research and Forecasting model coupled
111 with Chemistry (UI-WRF-Chem) by considering all potential sources of HONO
112 published in the literature. Since serious O_3 pollution and high soil emissions always
113 occurred in summer, a series of sensitivity experiments are conducted to quantify the
114 coupled and separate impact of SNO_x and SHONO on O_3 and secondary pollutants



115 during July over the North China, focusing on two city clusters, the Beijing-Tianjin-
116 Hebei (BTH) region and Fenwei Plain (FWP) region, both of which have the vast areas
117 of croplands and dense populations and experiencing severe O₃ and PM_{2.5} pollutions.
118 In addition, by quantitatively analyzing the difference in the response of surface O₃
119 concentrations and surface air temperature to the anthropogenic NO_x emissions
120 reductions in the presence vs. absence of soil Nr emissions, the roles of soil Nr
121 emissions on O₃ mitigation strategies and climate change are also studied. Our study is
122 designed to address the underestimated role of soil Nr emission in O₃ pollution, thereby
123 providing the scientific basis for O₃ mitigation strategies and climate change.

124 **2. Methodology**

125 **2.1 Model description**

126 **2.1.1 Model configurations, input data, and non-soil HONO emission**

127 The UI-WRF-Chem model, developed upon the standard version of WRF-Chem
128 3.8.1 (Grell et al., 2005), was used in this study. The 0.625°×0.5° Modern-Era
129 Retrospective analysis for Research and Applications, Version 2 (MERRA-2) reanalysis
130 data provide both the meteorological and chemical boundary and initial conditions
131 (Gelaro et al., 2017). The 0.25° × 0.25° Global Land Data Assimilation System
132 (GLDAS) data provides the initial and boundary conditions of soil properties, i.e., soil
133 moisture and temperature (Rodell, 2004). Details of Unified Inputs of meteorological
134 and chemical position data for UI-WRF-Chem, can be found in recent publications (Li
135 et al., 2024; Wang et al., 2023c). Anthropogenic emissions are imported from the Multi-
136 resolution Emission Inventory for China (MEIC: <http://www.meicmodel.org/>) with a



137 spatial resolution of $0.25^\circ \times 0.25^\circ$ for the year 2017. Biomass burning emissions are
138 from the Fire Inventory from NCAR version (FINN, version 1.5,
139 <https://www.acom.ucar.edu/Data/fire/>). Biogenic emissions are calculated using the
140 Model of Emissions of Gases and Aerosols from Nature (MEGAN) version 2.1
141 (Guenther et al., 2012).

142 The physical and chemical schemes include the Morrison 2-moment
143 microphysical scheme (Morrison et al., 2009), Grell 3-D cumulus scheme (Grell and
144 Dévényi, 2002), RRTMG for both longwave and shortwave radiation scheme (Iacono
145 et al., 2008), Yonsei University planetary boundary layer scheme (Hong, 2006), Noah
146 land surface model (Tewari, 2004), and the Carbon Bond Mechanism (CBMZ) for gas-
147 phase chemistry and the Model for Simulating Aerosol Interactions and Chemistry
148 (MOSAIC) aerosol module with four sectional aerosol bins and aqueous reactions
149 (Zaveri et al., 2008; Zaveri and Peters, 1999) are adopted in the UI-WRF-Chem model.
150 Two nested domains are used, domain one covers China with a horizontal resolution of
151 27 km and contains 112×112 grid cells, and domain two covers central and eastern
152 China and its surrounding area with a horizontal resolution of 9 km, containing
153 196×166 grid cells (study region are shown in Figure S1), both domains have 74 vertical
154 levels from surface to 50 hPa and 4 levels of soil. The simulations are conducted from
155 29th June to 31th July in 2018 with the first 2 days as the spin-up period. The model
156 outputs from 1th to 31th July in 2018 are analyzed.

157 The default WRF-Chem model only considers the gas-phase formation of HONO
158 ($\text{NO} + \text{OH} \rightarrow \text{HONO}$), thus underestimating the HONO concentrations. In this study, in



159 addition to considering SHONO (details in Section 2.1.2), potential sources of HONO
160 recognized in recent studies are also taken into account in the current model (Fu et al.,
161 2019; Li et al., 2010; Ye et al., 2016; Ye et al., 2017; Zhang et al., 2022b; Zhang et al.,
162 2022a; Zhang et al., 2016; Zhang et al., 2021; Zhang et al., 2020), including traffic
163 emissions, NO₂ heterogeneous reactions on ground and aerosol surfaces, and inorganic
164 nitrate photolysis in the atmosphere. Through a series of tests and comparisons with
165 observed surface HONO concentrations, the specific parameterization schemes of
166 HONO sources adopted in this study are shown in Text S1.

167 **2.1.2 Parameterization of soil Nr emissions**

168 The soil Nr emissions schemes in the UI-WRF-Chem model are updated in this
169 study. The default SNO_x scheme in UI-WRF-Chem, MEGAN v2.1, is replaced by the
170 Berkeley–Dalhousie–Iowa Soil NO Parameterization (BDISNP), and the
171 implementation of BDISNP can be found in Sha et al. (2021). Considering that the
172 baseline year of N fertilizer data is 2006, and the amount of N fertilizer application in
173 China has changed in the past ten years, we update the N fertilizer data to the year 2018
174 based on the N fertilizer application data at the province level from the statistical
175 yearbook (Table S1).

176 The process of soil HONO emission is similar to that of NO_x, as both are
177 influenced by the physical and chemical characteristics of soils. Consequently, soil
178 emissions of HONO with consideration of their dependence on land type, soil humidity,
179 and temperature are also parameterized into the UI-WRF-Chem model. We first map
180 the soil types measured in Oswald et al. (2013) (collected from 17 ecosystems in Table



181 S2) into the most closely matching MODIS land cover types in the model following
182 Feng et al. (2022a), described in Table S3. The optimal emission flux for each MODIS
183 land cover type is calculated as the average of the measured fluxes from the
184 category/categories in Oswald et al. (2013) that is/are been mapped into a specific
185 MODIS classification. We also collect the SHONO data from various ecosystems in
186 China published in different studies to correct the optimal SHONO fluxes in the model
187 (Table S4). These ecosystems include semi-arid, fertilized and irrigated farmland in
188 China. Consequently, the parameterization scheme takes into account the effect of
189 fertilizer application on the SHONO. After that, the optimal fluxes over the domains
190 are digested into the model and further scaled online according to the soil temperature
191 and water content in each model grid at each time step throughout the simulation period
192 by the following of equation from (Zhang et al., 2016):

$$193 \quad F_N(\text{HONO}) = F_{N,opt}(\text{HONO}) \cdot f(T) \cdot f(\text{SWC})$$

194 where $F_{N,opt}(\text{HONO})$ is the optimum flux of SHONO in terms of nitrogen. $f(T)$ and
195 $f(\text{SWC})$ are the scaling factors of soil temperature (T) and water content (SWC).

$$196 \quad f(T) = e^{\frac{E_a}{R} \left(\frac{T}{T_{opt}} - 1 \right)}$$

197 E_a is the activation energy of HONO (80 kJ mol⁻¹), R is the gas constant, T_{opt} is
198 the temperature at which optimum flux is emitted (298.15 K), T is the soil temperature
199 calculated online by the model, $f(\text{SWC})$ is fitted based on the data curves in Figures
200 1 and 3 in (Oswald et al., 2013) and the equation is as follows:

$$201 \quad f(\text{SWC}) = 1.04 \times \exp\left(-e^{\frac{\text{SWC}-11.32586}{5.27335} - \frac{\text{SWC}-11.32586}{5.27335} + 1}\right)$$

202 2.2 Model experiment design



203 The descriptions of the sensitivity simulations are shown in Table S5. Default
204 simulation uses MEGAN scheme to estimate SNO_x and no SHONO is considered. Base
205 simulation uses soil Nr emissions schemes with the improvement of using BDISNP
206 scheme for SNO_x and consideration of SHONO and other four HONO sources (as
207 described above). Comparison of results from Default and Base simulations is used to
208 show the improvement in the model performance after updating the soil Nr emissions
209 schemes and incorporating HONO potential sources. To explore the impact of soil Nr
210 emissions on O₃ and secondary pollutants, we conduct a series of sensitivity simulations
211 with soil NO_x and HONO emissions turned on/off separately and jointly (anthropogenic
212 emissions for the year 2017), i.e., NoSoilNr, NoSHONO and NoSNO_x. To evaluate the
213 role of soil Nr emissions on O₃ mitigation strategies and air temperature change under
214 different anthropogenic emission reduction scenarios, we further conduct the
215 Base_redANO_x and NoSoil_redANO_x simulations with anthropogenic NO_x emissions
216 reduced by 20%, 40%, 60%, 80% and 100%, respectively.

217 **2.3 Observational data**

218 The tropospheric column densities of NO₂ from TROPOMI (TROPOspheric
219 Monitoring Instrument) level-2 in version 1 with the horizontal spatial resolution of 3.5
220 × 7 km² are used. The quality controls, i.e., cloud-screened (cloud fraction below 30%)
221 and quality-assured (qa_value above 0.50), and averaging kernels (AK) are applied in
222 the comparison of the TROPOMI and UI-WRF-Chem simulated tropospheric NO₂
223 vertical column densities (defined as NO₂ VCD).

224 To evaluate the model performance on simulating surface air pollutants, we use



225 the hourly surface O₃ concentrations at 888 monitoring sites from the China National
226 Environmental Monitoring Center (CNEMC), and hourly surface HONO
227 concentrations measured by the In-situ Gas and Aerosol Compositions monitor (IGAC)
228 (Zhan et al., 2021) at Nanjing University of Information Science & Technology (NUIST)
229 (32.2° N, 118.7° E; 22m above sea level) (Xu et al., 2019).

230 **3. Results and discussions**

231 **3.1 Soil nitrogen emissions and air pollution evaluation**

232 Figure 1 shows the spatial distribution of simulated monthly mean SNO_x and
233 SHONO fluxes in July 2018 across North China. In most regions, SNO_x flux is nearly
234 doubled that of SHONO, and higher SNO_x and SHONO are concentrated in areas
235 dominated by cropland. The monthly total soil emissions over the whole study domain
236 (cropland) are 104.5 (82.4) Gg N mon⁻¹ for NO_x and 52.7 (45.9) Gg N mon⁻¹ for HONO.
237 In the densely populated BTH region, the monthly total SNO_x are 18.7 Gg N mon⁻¹,
238 which is equivalent to 37.3% of anthropogenic NO_x emissions for the year 2017. For
239 the FEW region, where also experiences severe O₃ and PM_{2.5} pollution, the monthly
240 total SNO_x (7.0 Gg N mon⁻¹) account for 29.2% of anthropogenic NO_x emissions. The
241 monthly total SHONO in both study regions are much lower than their SNO_x
242 counterparts, with the emissions of 6.9 and 4.6 Gg N mon⁻¹, accounting for 13.5% and
243 19.2% of anthropogenic NO_x emissions in BTH and FWP regions, respectively.

244 To evaluate the model performance, Figure 2 shows the tropospheric NO₂ VCD
245 from TROPOMI satellite products and UI-WRF-Chem simulations (Default and Base)
246 during July 2018 in North China. Default and Base can both reproduce the hot spots of



247 NO₂ VCD in urban areas shown in the TROPOMI observations. However, the Default
248 significantly underestimates the NO₂ VCD, especially in regions surrounding urban
249 areas. It is found that Default underestimates NO₂ VCD by 48% over the regions where
250 soil emissions dominate (i.e., soil Nr emissions contribute more than half to the
251 atmospheric nitrogen emissions), while the Base reduced the bias to 13% (Figure S2).
252 Overall, Base shows the improved performance in simulating NO₂ VCD in comparison
253 to Default with a decreasing bias from -30% (-21%) to +4% (+17%) in the study region
254 (cropland). The overestimated NO₂ VCD in Base is most likely attributed to the time
255 lag in anthropogenic emissions inventory used in the study (Chen et al., 2021),
256 uncertainties in the stratospheric portion of NO₂ VCD and AK caused the retrieval
257 errors (Van Geffen et al., 2020). Additionally, the estimated SNO_x are also subjected to
258 certain limitations and uncertainties. The first uncertainty comes from the amount of N
259 fertilizer application, which has been identified as the dominant contributor to SNO_x.
260 In this study, we use the amount of agricultural N fertilizer application at the province
261 level from the statistical yearbook to update the default N fertilizer application data in
262 the model (the baseline year for 2006), but a recent study showed that compound
263 fertilizer, usually with nitrogen (N), phosphorus (P), and potassium (K), were more
264 commonly used in China; if only N fertilizer is considered to nudge the N fertilizer
265 application data in the model, the estimated SNO_x may be underestimated by 11.1%–
266 41.5% (Huang et al., 2023). Furthermore, although we use the modeled green
267 vegetation fraction (GVF) to determine the distribution of arid (GVF ≤ 30%) and non-
268 arid (GVF > 30%) regions. Huber et al. (2023) showed that the estimated SNO_x based



269 on the static classification of arid vs. non-arid is very sensitive to the soil moisture, and
270 thus could not produce self-consistent results when using different input soil moisture
271 products unless a normalized soil moisture index to represent. Therefore, more direct
272 measurements of soil Nr fluxes are crucial to better constrain soil emissions and
273 improve the parametrization in the model.

274 We evaluate the simulation with the surface O₃ observations from the China
275 National Environmental Monitoring Centre (CNEMC) network
276 (<http://www.cnemc.cn/en/>) (Figure 3). Over the whole study region, the Base can better
277 capture the spatial distribution of observed surface MDA8 O₃ with a relatively higher
278 spatial correlation of $R = 0.68$ than that in Default ($R = 0.46$). The simulated monthly
279 averaged MDA8 O₃ concentrations across the 888 sites in the study region are 123.0 μg
280 m^{-3} in Default and 132.5 $\mu\text{g} \text{m}^{-3}$ in Base, respectively, which are both slightly higher
281 than the observed concentrations (120.7 $\mu\text{g} \text{m}^{-3}$). Overprediction is also observed for
282 the FWP and BTH regions in the Base simulation, with the normalized mean bias (NMB)
283 of 6.1% and 4.9%, respectively (Figure S3). These positive biases are mainly due to
284 overestimated transport of boundary O₃ in both horizontal and vertical directions
285 (Huang et al., 2023) and underestimated precipitation and cloud cover in the current
286 model (Sun et al., 2019).

287 We also compare the simulated surface HONO and nitrate concentrations to the
288 observations at a rural station in Nanjing during July 2018. Figure 4 shows that the
289 simulated HONO concentrations in Default are 98.3% lower than the observations. In
290 comparison, the Base with considering SHONO and other HONO potential sources



291 significantly improves the simulation performance and reduces the bias to 47.8%, and
292 also reproduces the diurnal variation of HONO with the temporal correlation of $R =$
293 0.76. It is worth noting that the concentrations of HONO from 08 am to 18 pm are lower
294 than the observations, this discrepancy may be attributed to the underestimated
295 contribution from the predominant sources of HONO during the daytime, such as NO₂
296 heterogeneous reactions on ground and aerosol surfaces. Moreover, the contributions
297 of different sources to ambient HONO concentrations at this rural station are also
298 evaluated, the soil emissions could contribute almost 25.8% to the surface HONO,
299 which may be partially attributed to the high emissions of HONO from croplands
300 around the city of Nanjing (Figure S4). The results that soil emissions contribute less
301 to the daytime positive flux than the other source is consistent with previous studies
302 (Skiba et al., 2020; Wang et al., 2023b). For nitrate concentration, the Base simulation
303 shows a lower bias (5.6%) and an improved diurnal variation (temporal correlation of
304 $R = 0.92$) compared to the Default simulation (bias = 27.8%, $R = 0.85$). We
305 acknowledge that there are certain uncertainties in the current model. Nevertheless, the
306 improved simulation performance compared to the Default illustrates the credibility of
307 the results obtained from the Base simulation.

308 **3.2 Impact on O₃ formation and air quality**

309 To quantify the effects of SNO_x and SHONO on atmospheric oxidation capacity,
310 O₃ formation and air quality as well as their combined effect, the conventional brute-
311 force method was used, i.e., the impact of a specific source is determined in atmospheric
312 chemistry models as the differences between the standard/base simulation with all



313 emissions turned on and a sensitivity simulation with this source turned off or perturbed
314 (Table S5). As shown in Figure 5, the contribution of SNO_x and SHONO to surface
315 NO₂ and HONO has a different spatial pattern from that of the fluxes of SNO_x and
316 SHONO. Overall, the maximum contribution of SNO_x to the monthly average surface
317 NO₂ concentrations is 78.6%, with a domain-averaged value of 30.3%. Regionally,
318 SNO_x contribute 5.5 μg m⁻³ (37.1%) and 2.5 μg m⁻³ (31.8%) to the surface NO₂ in the
319 BTH and FWP regions, respectively, which are both higher than the domain-averaged
320 contribution. Although SHONO fluxes are lower than that of SNO_x, its effect on
321 ambient HONO cannot be ignored. Over the study region, the contribution of SHONO
322 to surface HONO concentration ranges from 0 to 49.0%, with a domain-averaged value
323 of 35.6%. For the selected key regions, there are 1.8 μg/m³ (36.7%) and 1.5 μg/m³
324 (38.0%) of the monthly average HONO concentrations in the BTH and FWP regions,
325 respectively, from soil emissions. It is noteworthy that, despite the surface NO₂ (HONO)
326 concentrations in the study regions being impacted by less than 13% (17%) due to
327 SHONO (SNO_x), the combined effects of soil Nr emissions on surface NO₂ (HONO)
328 are found to be greater than the individual effects, which are 38.4% (40.3%) for BTH
329 and 33.9% (40.1%) for FWP region, respectively (Table S6). These results highlight the
330 importance of considering the cumulative impacts of multiple reactive nitrogen
331 emissions from soils on air pollution.

332 Consequently, substantial soil Nr emissions have a non-negligible effect on
333 atmospheric oxidation and the formation of secondary pollutants. For atmospheric
334 oxidation, we assess the impact of soil Nr emission on the maximum 1 h (max-1h) ·OH



335 levels and find that SHONO have a potential to increase the max-1h $\cdot\text{OH}$ in most areas,
336 with a domain-averaged increase of 10.0%. On the contrary, the inclusion of SNO_x
337 results in a significant reduction of 31.3% in the max-1h $\cdot\text{OH}$ across the entire study
338 domain. Considering the combined effect of SNO_x and SHONO, there is an overall
339 decrease of 24.3% in the max-1h $\cdot\text{OH}$ over the study domain, with the BTH region
340 experiencing a decrease of 22.6% and FWP region showing a relatively greater
341 reduction of 32.2% (Table S7). These findings are different from the previous study,
342 which showed that soil background emissions including NO_x and HONO led to a 7.5%
343 increase in max-1h $\cdot\text{OH}$ in China (Wang et al., 2023b). We stress the crucial role of
344 SNO_x in influencing $\cdot\text{OH}$ concentrations and highlight the varying impacts across
345 different regions. For secondary pollutants, substantial O_3 enhancement is found in
346 Henan and Hubei provinces, while the increase in nitrate is consistent with the spatial
347 pattern of surface NO_2 from soil emissions. Specifically, soil Nr emissions increase the
348 monthly average MDA8 O_3 and nitrate concentrations by 18.2% and 31.8%,
349 respectively, across the study domain, with the increase of 16.9% and 42.4% in the BTH
350 region and 17.2% and 42.7% in the FWP region. Moreover, soil emissions of NO_x have
351 a stronger effect on O_3 and nitrate in North China than those of SHONO.

352 The ratio of surface H_2O_2 to HNO_3 concentrations (hereafter $\text{H}_2\text{O}_2/\text{HNO}_3$) was
353 used as an indicator of the O_3 formation regime to study the changes in sensitivity of
354 summer O_3 to its precursors after considering the soil Nr emissions. The threshold of
355 $\text{H}_2\text{O}_2/\text{HNO}_3$ for determining O_3 formation regime varies regionally (Sillman, 1995),
356 thus in this study, we identify the regions with $\text{H}_2\text{O}_2/\text{HNO}_3$ values greater than 0.65 as



357 NO_x-sensitive regime, H₂O₂/HNO₃ values lower than 0.35 as VOCs-sensitive regime,
358 and H₂O₂/HNO₃ values between 0.35 and 0.65 as VOCs-NO_x mixed sensitive regime
359 (Shen et al., 2023). Figure 6 illustrates that the majority of BTH region has H₂O₂/HNO₃
360 values lower than 0.35 in Base simulation, indicating a VOCs-sensitive regime or NO_x-
361 saturated regime, which is consistent with the previous studies based on satellite
362 observations and model simulations (Wang et al., 2019; Wang et al., 2017). The
363 distribution of sensitivity of O₃ to precursor emission in FWP regions are more complex
364 with a mix of three O₃ formation regimes, which is attributed to the large population,
365 regional urbanization and industrialization. However, when soil nitrogen emissions are
366 excluded, the H₂O₂/HNO₃ values mostly increase within 40% and the O₃ formation
367 regime shifts to VOCs-NO_x mixed sensitive regime and NO_x-sensitive regime in both
368 BTH and FWP regions. Although soil Nr emissions are lower than anthropogenic
369 emissions, they still could affect the sensitivity of O₃ to its precursors and thus have an
370 impact on the effectiveness of emission reduction policies. Therefore, soil emissions
371 must be considered in formatting policies for the prevention and management of O₃
372 pollution.

373 **3.3 Implication on O₃ mitigation strategies and temperature rise**

374 Due to the influence of soil Nr emissions, the sensitivity of O₃ pollution to its
375 precursors varies spatially, depending on the local levels of anthropogenic emissions. It
376 is thus important to quantify the role of soil Nr emissions in O₃ pollution regulation for
377 improving the effectiveness of air control measures. We conduct a series of sensitivity
378 experiments with anthropogenic NO_x emissions reduced by 20%, 40%, 60%, 80% and



379 100%, respectively, relative to the Base simulation (Table S5), and analyze the
380 difference in the response of surface O₃ concentrations to the anthropogenic NO_x
381 emissions reductions in the presence and absence of soil Nr emissions. Figure 7 shows
382 that with the reduction of anthropogenic NO_x emissions, MDA8 O₃ concentrations show
383 an accelerated decreasing trend, suggesting increasing efficiency of anthropogenic NO_x
384 control measures. And MDA8 O₃ response to anthropogenic NO_x emissions in the BTH
385 region is more curved (nonlinear) than that in the FWP region, which is consistent with
386 the fact that the BTH tends to have more NO_x-saturated O₃ production (Figure 6).

387 It is noted that the reduction of anthropogenic NO_x emissions in the presence of
388 soil Nr emissions leads to a slower decrease in MDA8 O₃ compared to when soil Nr
389 emissions are excluded. We further analyze the details of the domain-averaged MDA8
390 O₃ changes under different anthropogenic reduction scenarios for the two key regions.
391 Specifically, in the BTH region, MDA8 O₃ decrease by 1.3% (1.8 μg m⁻³), 3.4% (4.6
392 μg m⁻³), 6.3% (8.7 μg m⁻³), 10.7% (14.7 μg m⁻³), and 17.4% (24.0 μg m⁻³) with
393 anthropogenic NO_x emission reductions by 20%, 40%, 60%, 80%, and 100%,
394 respectively, in the present of soil Nr emissions. Comparatively, in the absence of soil
395 Nr emissions, the reductions in MDA8 O₃ are more pronounced and decrease by 2.3%
396 (2.7 μg m⁻³), 5.6% (6.6 μg m⁻³), 10.7% (12.8 μg m⁻³), 19.4% (23.2 μg m⁻³), and 42.3%
397 (50.6 μg m⁻³), respectively. In the FWP region, with a 20% reduction in anthropogenic
398 NO_x emissions, MDA8 O₃ levels only exhibit a slight decrease of 1.7% (2.3 μg m⁻³) in
399 the presence of soil Nr emissions, whereas a decrease of 2.3% (2.6 μg m⁻³) is found in
400 the absence of soil Nr emissions. When anthropogenic NO_x emissions are removed



401 entirely, MDA8 O₃ decreases by 13.6% (17.7 μg m⁻³) in the presence of soil Nr
402 emissions, and more significant decreases are found in the absent of soil Nr emissions
403 with a reduction of 27.4% (34.0 μg m⁻³) (as shown in Figure 7b-c, e-f). We conclude
404 that the existence of soil Nr emissions could contribute to an additional part of O₃
405 production, amounting to a range of 0-24.9% in the BTH and 0-13.8% in the FWP
406 region, and these suppressions could be enlarged over the rural areas where have more
407 substantial soil Nr emissions (e.g. 0-32.3% in cropland over the BTH and 0-15.0% in
408 croplands over the FWP region). These findings suggest that soil Nr emissions have the
409 potential to suppress the effectiveness of measures implemented to mitigate O₃
410 pollution, and this effect becomes more significant as anthropogenic emissions increase.

411 We also quantify the O₃ generated from soil Nr emission source (denoted as the
412 soil O₃) under the different anthropogenic NO_x emission scenarios. Overall, soil O₃
413 concentrations in croplands are higher than in non-croplands. Regionally, in the BTH
414 region, the soil O₃ concentrations are 19.8 μg m⁻³ under high anthropogenic emissions
415 level (referred to as the Base simulation), while the soil O₃ concentrations significantly
416 increase to 46.4 μg m⁻³ when all anthropogenic NO_x emissions are cut down (shown as
417 red bar in Figure 7b). A similar trend is also found in the FWP region, although soil O₃
418 concentrations are relatively lower than that in the BTH region, the soil O₃
419 concentrations are 19.0 μg m⁻³ in the Base simulation, and do not change significantly
420 with the reduction of anthropogenic emissions, but increase to 31.9 μg m⁻³ when
421 anthropogenic NO_x emissions are excluded (shown as red bar in Figure 7c). The
422 reduction in anthropogenic NO_x emissions results in a shift of the O₃ formation regime



423 towards a more NO_x -sensitive chemical regime, leading to a higher contribution of O_3
424 from soil sources. We conclude that with stricter anthropogenic emission reduction
425 measures, the contributions of soil Nr emissions to O_3 production in both absolute and
426 relative value would increase and further hamper the effectiveness of anthropogenic
427 emission reductions. To effectively mitigate the desired level of O_3 concentrations, it is
428 necessary to implement much stricter control measures for anthropogenic emissions
429 due to the synergistic effects of SNO_x and SHONO .

430 Here we show that the substantial soil Nr emissions present an additional challenge
431 for O_3 pollution regulation in the North China. We further assess the impact of soil Nr
432 emissions on air temperature change under different anthropogenic emission reduction
433 scenarios. By comparing changes in air temperature at 2m (T_2) with and without soil
434 Nr emissions under different anthropogenic emission reduction scenarios, Figure 8
435 shows that incorporating soil Nr emissions results in a slower rate of T_2 increase
436 compared to scenarios without soil Nr emissions, and this phenomenon is consistent
437 across all study regions. In the FWP region, when anthropogenic NO_x emissions are
438 eliminated, T_2 increases by $0.056\text{ }^\circ\text{C}$ in the presence of soil Nr emissions, compared to
439 $0.092\text{ }^\circ\text{C}$ in the absence of soil Nr emissions. In the BTH region, which has relatively
440 high anthropogenic emissions, reducing anthropogenic NO_x emissions by the same
441 proportion could result in relatively greater warming, and T_2 increases by $0.084\text{ }^\circ\text{C}$ in
442 the presence of soil Nr emissions, compared to $0.15\text{ }^\circ\text{C}$ in the absence of soil Nr
443 emissions when anthropogenic NO_x emissions are excluded. This is attributed to
444 aerosols (such as sulfate and nitrate) and NO_x emissions and their effective radiative



445 forcing (ERF) associated with a cooling effect (high confidence) (Liao and Xie, 2021;
446 Bellouin et al., 2020). Decreases in aerosol concentrations and NO_x emissions could
447 weaken the cooling effect and potentially accelerate warming to some extent, while soil
448 Nr emissions can offset temperature rise caused by declining anthropogenic NO_x
449 emissions (Figure S5). Therefore, although soil Nr emissions are relatively low
450 compared to anthropogenic emissions, the combined effects of NO_x and HONO
451 emissions from natural soil and agricultural land should be considered when assessing
452 climate change and implementing strategies to mitigate O₃ pollution.

453 **4. Conclusions**

454 In this study, the updated soil Nr emission scheme was implemented in the UI-
455 WRF-Chem model and used to estimate the combined and individual impact of SNO_x
456 and SHONO on subsequent changes in air quality and air temperature rise in North
457 China, with a focus on two key regions (the BTH and FWP regions) because of high
458 levels of soil Nr and anthropogenic emissions. We show that the SNO_x flux is nearly
459 doubled that of SHONO during July 2018, with higher soil emissions in areas with
460 extensive cropland. The contribution of soil Nr emissions to average surface NO₂ and
461 HONO are 38.4% and 40.3% in the BTH, and 33.9% and 40.1% in the FWP region,
462 respectively, and the substantial soil Nr emissions lead to a considerable increase in the
463 monthly average MDA8 O₃ and nitrate concentrations, with the values of 16.9% and
464 42.4% in the BTH region and 17.2% and 42.7% in the FWP region, which both exceed
465 the individual SNO_x or SHONO effect. The presence of soil Nr emissions, acting as
466 precursors of O₃ and secondary inorganic aerosols, has a suppressing effect on efforts



467 to mitigate O₃ pollution, particularly in the BTH region, and also leads to a slower
468 increase rate of T2 compared to scenarios without soil Nr emissions. We note that the
469 effect of soil Nr emissions shows spatial heterogeneity under different anthropogenic
470 NO_x emissions reduction scenarios.

471 However, we admit that uncertainties in both soil Nr and anthropogenic emissions,
472 as well as the parameterization scheme of HONO sources. The agricultural emissions
473 of another important reactive nitrogen gas, NH₃, may also be underestimated due to
474 uncertainties in agricultural fertilizer application and livestock waste in MEIC
475 inventory (Li et al., 2021a). These uncertainties could impact the aerosol formation and
476 local cooling effect. Also, the discrepancies between simulated and observed NO₂, O₃
477 and other air pollutants in the model may affect the assessment of the role of soil Nr
478 emissions in O₃ mitigation strategies and their impact on climate change. Thus, more
479 direct measurements of soil Nr fluxes are crucial to better constrain soil emissions and
480 improve the parametrization in the model.

481 Our study highlights that despite soil Nr emissions being lower than anthropogenic
482 emissions, they still have a substantial impact on the effectiveness of O₃ pollution
483 mitigation measures, and this effect becomes more significant as anthropogenic
484 emissions decrease. Therefore, reactive nitrogen from soil emission source must be
485 considered in formatting measures for the prevention and management of O₃, as well
486 as addressing climate change.

487



488 **Code and data availability.** Some of the data repositories have been listed in Section 2.
489 The other data, model outputs and codes can be accessed by contacting Tong Sha via
490 tong-sha@sust.edu.cn.

491 **Author contributions.** TS performed the model simulation, data analysis and
492 manuscript writing. TS and JW proposed the idea. SY, QC and LL supervised this work
493 and revised the manuscript. XM, ZF and KB helped the revision of the manuscript. YZ
494 provided and analyzed the observation data.

495 **Competing interests.** The authors declare that they have no conflict of interest.

496 **Acknowledgements.** This study is supported by the National Natural Science
497 Foundation of China (grant nos. 42205107, 42130714). Jun Wang's participation is
498 made possible via the in-kind support from the University of Iowa.

499

500 **References**

- 501 TROPOMI ATBD of the total and tropospheric NO₂ data products.
502 Almaraz, M., Bai, E., Wang, C., Trousdell, J., Conley, S., Faloon, I., & Houlton, B. Z.:
503 Agriculture is a major source of NO_x pollution in California, *Sci. Adv.*, 4(1),
504 eaao3477., 2018.
505 Bellouin, N., Quaas, J., Gryspeerdt, E., Kinne, S., Stier, P., Watson-Parris, D., Boucher,
506 O., Carslaw, K. S., Christensen, M., and Daniaou, A. L.: Bounding global aerosol
507 radiative forcing of climate change, *Rev. Geophys.*, 58, e2019RG000660, 2020.
508 Chen, K., Wang, P., Zhao, H., Wang, P., Gao, A., Myllyvirta, L., and Zhang, H.:
509 Summertime O₃ and related health risks in the north China plain: A modeling study
510 using two anthropogenic emission inventories, *Atmos. Environ.*, 246, 118087,
511 10.1016/j.atmosenv.2020.118087, 2021.
512 Elshorbany, Y. F., Steil, B., Brühl, C., and Lelieveld, J.: Impact of HONO on global
513 atmospheric chemistry calculated with an empirical parameterization in the



- 514 EMAC model, *Atmos. Chem. Phys.*, 12, 9977-10000, 10.5194/acp-12-9977-2012,
515 2012.
- 516 Feng, T., Zhao, S., Liu, L., Long, X., Gao, C., and Wu, N.: Nitrous acid emission from
517 soil bacteria and related environmental effect over the North China Plain,
518 *Chemosphere*, 287, 132034, 10.1016/j.chemosphere.2021.132034, 2022a.
- 519 Feng, Z., Xu, Y., Kobayashi, K., Dai, L., Zhang, T., Agathokleous, E., Calatayud, V.,
520 Paoletti, E., Mukherjee, A., Agrawal, M., Park, R. J., Oak, Y. J., and Yue, X.: Ozone
521 pollution threatens the production of major staple crops in East Asia, *Nat. Food*, 3,
522 47-56, 10.1038/s43016-021-00422-6, 2022b.
- 523 Fu, X., Wang, T., Zhang, L., Li, Q., Wang, Z., Xia, M., Yun, H., Wang, W., Yu, C., Yue,
524 D., Zhou, Y., Zheng, J., and Han, R.: The significant contribution of HONO to
525 secondary pollutants during a severe winter pollution event in southern China,
526 *Atmos. Chem. Phys.*, 19, 1-14, 10.5194/acp-19-1-2019, 2019.
- 527 Gelaro, R., McCarty, W., Suárez, M. J., Todling, R., Molod, A., Takacs, L., Randles, C.
528 A., Darmenov, A., Bosilovich, M. G., Reichle, R., Wargan, K., Coy, L., Cullather,
529 R., Draper, C., Akella, S., Buchard, V., Conaty, A., da Silva, A. M., Gu, W., Kim,
530 G.-K., Koster, R., Lucchesi, R., Merkova, D., Nielsen, J. E., Partyka, G., Pawson,
531 S., Putman, W., Rienecker, M., Schubert, S. D., Sienkiewicz, M., and Zhao, B.:
532 The Modern-Era Retrospective Analysis for Research and Applications, Version 2
533 (MERRA-2), *J. Clim.*, 30, 5419-5454, 10.1175/jcli-d-16-0758.1, 2017.
- 534 Grell, G. A. and Dévényi, D.: A generalized approach to parameterizing convection
535 combining ensemble and data assimilation techniques, *Geophys. Res. Lett.*, 29,
536 10.1029/2002gl015311, 2002.
- 537 Grell, G. A., Peckham, S. E., Schmitz, R., McKeen, S. A., Frost, G., Skamarock, W. C.,
538 and Eder, B.: Fully coupled “online” chemistry within the WRF model, *Atmos.*
539 *Environ.*, 39, 6957-6975, 10.1016/j.atmosenv.2005.04.027, 2005.
- 540 Guenther, A. B., Jiang, X., Heald, C. L., Sakulyanontvittaya, T., Duhl, T., Emmons, L.
541 K., and Wang, X.: The Model of Emissions of Gases and Aerosols from Nature
542 version 2.1 (MEGAN2.1): an extended and updated framework for modeling
543 biogenic emissions, *Geosci. Model Dev.*, 5, 1471-1492, 10.5194/gmd-5-1471-



- 544 2012, 2012.
- 545 Hong, S. Y., Noh, Y., and Dudhia, J.: A new vertical diffusion package with an explicit
546 treatment of entrainment processes, *Mon. Weather Rev.*, 134 (9), 2318, 2006.
- 547 Huang, L., Fang, J., Liao, J., Yarwood, G., Chen, H., Wang, Y., and Li, L.: Insights into
548 soil NO emissions and the contribution to surface ozone formation in China,
549 *Atmos. Chem. Phys.*, 23, 14919-14932, 10.5194/acp-23-14919-2023, 2023.
- 550 Huang, Y., Hickman, J. E., and Wu, S.: Impacts of enhanced fertilizer applications on
551 tropospheric ozone and crop damage over sub-Saharan Africa, *Atmos. Environ.*,
552 180, 117-125, 10.1016/j.atmosenv.2018.02.040, 2018.
- 553 Huber, D. E., Steiner, A. L., and Kort, E. A.: Sensitivity of Modeled Soil NO_x Emissions
554 to Soil Moisture, *J. Geophys. Res.: Atmos.*, 128, 10.1029/2022jd037611, 2023.
- 555 Iacono, M. J., Delamere, J. S., Mlawer, E. J., Shephard, M. W., Clough, S. A., and
556 Collins, W. D.: Radiative forcing by long-lived greenhouse gases: Calculations
557 with the AER radiative transfer models, *J. Geophys. Res.: Atmos.*, 113,
558 10.1029/2008jd009944, 2008.
- 559 Li, B., Chen, L., Shen, W., Jin, J., Wang, T., Wang, P., Yang, Y., and Liao, H.: Improved
560 gridded ammonia emission inventory in China, *Atmos. Chem. Phys.*, 21, 15883-
561 15900, 10.5194/acp-21-15883-2021, 2021a.
- 562 Li, C., Wang, J., Zhang, H., Diner, D. J., Hasheminassab, S., and Janecek, N.:
563 Improvement of Surface PM_{2.5} Diurnal Variation Simulations in East Africa for
564 the MAIA Satellite Mission, *ACS ES&T Air*, 10.1021/acsestair.3c00008, 2024.
- 565 Li, G., Lei, W., Zavala, M., Volkamer, R., Dusanter, S., Stevens, P., and Molina, L. T.:
566 Impacts of HONO sources on the photochemistry in Mexico City during the
567 MCMA-2006/MILAGO Campaign, *Atmos. Chem. Phys.*, 10, 6551-6567,
568 10.5194/acp-10-6551-2010, 2010.
- 569 Li, K., Jacob, D. J., Shen, L., Lu, X., De Smedt, I., and Liao, H.: Increases in surface
570 ozone pollution in China from 2013 to 2019: anthropogenic and meteorological
571 influences, *Atmos. Chem. Phys.*, 20, 11423-11433, 10.5194/acp-20-11423-2020,
572 2020.
- 573 Li, K., Jacob, D. J., Liao, H., Zhu, J., Shah, V., Shen, L., Bates, K. H., Zhang, Q., and



- 574 Zhai, S.: A two-pollutant strategy for improving ozone and particulate air quality
575 in China, *Nat. Geosci.*, 12, 906-910, 10.1038/s41561-019-0464-x, 2019.
- 576 Li, K., Jacob, D. J., Liao, H., Qiu, Y., Shen, L., Zhai, S., Bates, K. H., Sulprizio, M. P.,
577 Song, S., Lu, X., Zhang, Q., Zheng, B., Zhang, Y., Zhang, J., Lee, H. C., and Kuk,
578 S. K.: Ozone pollution in the North China Plain spreading into the late-winter haze
579 season, *Proc. Natl. Acad. Sci. U.S.A.*, 118, 10.1073/pnas.2015797118, 2021b.
- 580 Liao, H. and Xie, P.: The roles of short-lived climate forcers in a changing climate, *Adv.*
581 *Clim. Change Res.*, 17, 685, 2021.
- 582 Liu, X., Zhang, Y., Han, W., Tang, A., Shen, J., Cui, Z., Vitousek, P., Erisman, J. W.,
583 Goulding, K., Christie, P., Fangmeier, A., and Zhang, F.: Enhanced nitrogen
584 deposition over China, *Nature*, 494, 459-462, 10.1038/nature11917, 2013.
- 585 Liu, Y. and Wang, T.: Worsening urban ozone pollution in China from 2013 to 2017 –
586 Part 2: The effects of emission changes and implications for multi-pollutant
587 control, *Atmos. Chem. Phys.*, 20, 6323-6337, 10.5194/acp-20-6323-2020, 2020a.
- 588 Liu, Y. and Wang, T.: Worsening urban ozone pollution in China from 2013 to 2017 –
589 Part 1: The complex and varying roles of meteorology, *Atmos. Chem. Phys.*, 20,
590 6305-6321, 10.5194/acp-20-6305-2020, 2020b.
- 591 Lu, C. and Tian, H.: Global nitrogen and phosphorus fertilizer use for agriculture
592 production in the past half century: shifted hot spots and nutrient imbalance, *Earth*
593 *Syst. Sci. Data*, 9, 181-192, 10.5194/essd-9-181-2017, 2017.
- 594 Lu, X., Zhang, L., Chen, Y., Zhou, M., Zheng, B., Li, K., Liu, Y., Lin, J., Fu, T.-M., and
595 Zhang, Q.: Exploring 2016–2017 surface ozone pollution over China: source
596 contributions and meteorological influences, *Atmos. Chem. Phys.*, 19, 8339-8361,
597 10.5194/acp-19-8339-2019, 2019.
- 598 Lu, X., Ye, X., Zhou, M., Zhao, Y., Weng, H., Kong, H., Li, K., Gao, M., Zheng, B.,
599 Lin, J., Zhou, F., Zhang, Q., Wu, D., Zhang, L., and Zhang, Y.: The
600 underappreciated role of agricultural soil nitrogen oxide emissions in ozone
601 pollution regulation in North China, *Nat. Commun.*, 12, 10.1038/s41467-021-
602 25147-9, 2021.
- 603 Morrison, H., Thompson, G., and Tatarskii, V.: Impact of Cloud Microphysics on the



- 604 Development of Trailing Stratiform Precipitation in a Simulated Squall Line:
605 Comparison of One- and Two-Moment Schemes, *Mon. Weather Rev.*, 137, 991-
606 1007, 10.1175/2008mwr2556.1, 2009.
- 607 Oswald, R., Behrendt, T., Ermel, M., Wu, D., Su, H., Cheng, Y., Breuninger, C.,
608 Moravek, A., Mougín, E., Delon, C., Loubet, B., Pommerening-Röser, A., Sörgel,
609 M., Pöschl, U., Hoffmann, T., Andreae, M. O., Meixner, F. X., and Trebs, I.:
610 HONO Emissions from Soil Bacteria as a Major Source of Atmospheric Reactive
611 Nitrogen, *Science*, 341, 1233-1235, 10.1126/science.1242266, 2013.
- 612 Pinder, R. W., Davidson, E. A., Goodale, C. L., Greaver, T. L., Herrick, J. D., and Liu,
613 L.: Climate change impacts of US reactive nitrogen, *Proc. Natl. Acad. Sci. U.S.A.*,
614 109, 7671-7675, 10.1073/pnas.1114243109, 2012.
- 615 Reay, D. S., Dentener, F., Smith, P., Grace, J., and Feely, R. A.: Global nitrogen
616 deposition and carbon sinks., *Nat. Geosci.*, 1(7), 430-437, 2008.
- 617 Rodell, M. H., P. R.; Jambor, U.; Gottschalck, J.; Mitchell, K.; Meng, C.-J.; Arsenault,
618 K.; Cosgrove, B.; Radakovich, J.; Bosolovich, M.; Entin, J. K.; Walker, J. P.;
619 Lohmann, D.; D., T. : The global land data assimilation system., *Bull. Am.*
620 *Meteorol. Soc.*, 85 (3), 381-394., 2004.
- 621 Romer, P. S., Duffey, K. C., Wooldridge, P. J., Edgerton, E., Baumann, K., Feiner, P. A.,
622 Miller, D. O., Brune, W. H., Koss, A. R., de Gouw, J. A., Misztal, P. K., Goldstein,
623 A. H., and Cohen, R. C.: Effects of temperature-dependent NO_x emissions on
624 continental ozone production, *Atmos. Chem. Phys.*, 18, 2601-2614, 10.5194/acp-
625 18-2601-2018, 2018.
- 626 Sha, T., Ma, X., Zhang, H., Janecek, N., Wang, Y., Wang, Y., Castro García, L.,
627 Jenerette, G. D., and Wang, J.: Impacts of Soil NO_x Emission on O₃ Air Quality in
628 Rural California, *Environ. Sci. Technol.*, 55, 7113-7122, 10.1021/acs.est.0c06834,
629 2021.
- 630 Shen, Y., Xiao, Z., Wang, Y., Xiao, W., Yao, L., and Zhou, C.: Impacts of Agricultural
631 Soil NO_x Emissions on O₃ Over Mainland China, *J. Geophys. Res.: Atmos.*, 128,
632 10.1029/2022jd037986, 2023.
- 633 Sillman, S.: The use of NO_y, H₂O₂, and HNO₃ as indicators for ozone-NO_x-hydrocarbon



- 634 sensitivity in urban locations., *J. Geophys. Res.*, 100(D7), 14175–14188.,
635 <https://doi.org/10.1029/94JD02953>, 1995.
- 636 Skiba, U., Medinets, S., Cardenas, L. M., Carnell, E. J., Hutchings, N., and Amon, B.:
637 Assessing the contribution of soil NO_x emissions to European atmospheric
638 pollution, *Environ. Res. Lett.*, 10.1088/1748-9326/abd2f2, 2020.
- 639 Sun, L., Xue, L., Wang, Y., Li, L., Lin, J., Ni, R., Yan, Y., Chen, L., Li, J., Zhang, Q.,
640 and Wang, W.: Impacts of meteorology and emissions on summertime surface
641 ozone increases over central eastern China between 2003 and 2015, *Atmos. Chem.*
642 *Phys.*, 19, 1455-1469, 10.5194/acp-19-1455-2019, 2019.
- 643 Tan, W., Wang, H., Su, J., Sun, R., He, C., Lu, X., Lin, J., Xue, C., Wang, H., Liu, Y.,
644 Liu, L., Zhang, L., Wu, D., Mu, Y., and Fan, S.: Soil Emissions of Reactive
645 Nitrogen Accelerate Summertime Surface Ozone Increases in the North China
646 Plain, *Environ. Sci. Technol.*, 57, 12782-12793, 10.1021/acs.est.3c01823, 2023.
- 647 Tewari, M., Chen F., Wang W., Dudhia J., LeMone M. A., Mitchell K., M. Gayno Ek,
648 Wegiel G., J., and Cuenca R. H.: Implementation and verification of the unified
649 NOAA land surface model in the WRF model, in 20th Conference on Weather
650 Analysis and Forecasting/16th Conference on Numerical Weather Prediction, 11–
651 15., 2004.
- 652 Turner, M. C., Jerrett, M., Pope, C. A., Krewski, D., Gapstur, S. M., Diver, W. R.,
653 Beckerman, B. S., Marshall, J. D., Su, J., Crouse, D. L., and Burnett, R. T.: Long-
654 Term Ozone Exposure and Mortality in a Large Prospective Study, *Am. J. Resp.*
655 *Crit. Care.*, 193, 1134-1142, 10.1164/rccm.201508-1633OC, 2016.
- 656 Unger, N., Zheng, Y., Yue, X., and Harper, K. L.: Mitigation of ozone damage to the
657 world's land ecosystems by source sector, *Nat. Clim. Change*, 10, 134-137,
658 10.1038/s41558-019-0678-3, 2020.
- 659 van Geffen, J., Boersma, K. F., Eskes, H., Sneep, M., ter Linden, M., Zara, M., and
660 Veefkind, J. P.: S5P TROPOMI NO₂ slant column retrieval: method, stability,
661 uncertainties and comparisons with OMI, *Atmos. Meas. Tech.*, 13, 1315-1335,
662 10.5194/amt-13-1315-2020, 2020.
- 663 Vinken, G. C. M., Boersma, K. F., Maasakkers, J. D., Adon, M., and Martin, R. V.:



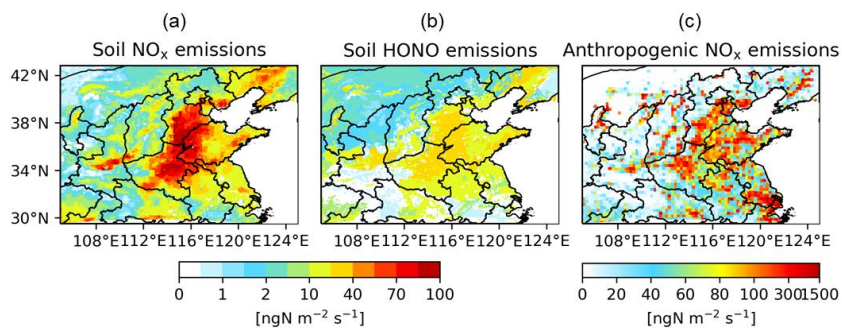
- 664 Worldwide biogenic soil NO_x emissions inferred from OMI NO₂ observations,
665 Atmos. Chem. Phys., 14, 10363-10381, 10.5194/acp-14-10363-2014, 2014.
- 666 Wang, N., Lyu, X., Deng, X., Huang, X., Jiang, F., and Ding, A.: Aggravating O₃
667 pollution due to NO_x emission control in eastern China, Sci. Total Environ., 677,
668 732-744, 10.1016/j.scitotenv.2019.04.388, 2019.
- 669 Wang, Q. g., Han, Z., Wang, T., and Zhang, R.: Impacts of biogenic emissions of VOC
670 and NO_x on tropospheric ozone during summertime in eastern China, Sci. Total
671 Environ., 395, 41-49, 10.1016/j.scitotenv.2008.01.059, 2008.
- 672 Wang, R., Bei, N., Wu, J., Li, X., Liu, S., Yu, J., Jiang, Q., Tie, X., and Li, G.: Cropland
673 nitrogen dioxide emissions and effects on the ozone pollution in the North China
674 plain, Environ. Pollut., 294, 118617, 10.1016/j.envpol.2021.118617, 2022a.
- 675 Wang, R., Bei, N., Pan, Y., Wu, J., Liu, S., Li, X., Yu, J., Jiang, Q., Tie, X., and Li, G.:
676 Urgency of controlling agricultural nitrogen sources to alleviate summertime air
677 pollution in the North China Plain, Chemosphere, 311, 137124,
678 10.1016/j.chemosphere.2022.137124, 2023a.
- 679 Wang, T., Xue, L., Brimblecombe, P., Lam, Y. F., Li, L., and Zhang, L.: Ozone pollution
680 in China: A review of concentrations, meteorological influences, chemical
681 precursors, and effects, Sci. Total Environ., 575, 1582-1596,
682 10.1016/j.scitotenv.2016.10.081, 2017.
- 683 Wang, W., Parrish, D. D., Wang, S., Bao, F., Ni, R., Li, X., Yang, S., Wang, H., Cheng,
684 Y., and Su, H.: Long-term trend of ozone pollution in China during 2014–2020:
685 distinct seasonal and spatial characteristics and ozone sensitivity, Atmos. Chem.
686 Phys., 22, 8935-8949, 10.5194/acp-22-8935-2022, 2022b.
- 687 Wang, Y., Ge, C., Castro Garcia, L., Jenerette, G. D., Oikawa, P. Y., and Wang, J.:
688 Improved modelling of soil NO_x emissions in a high temperature agricultural
689 region: role of background emissions on NO₂ trend over the US, Environ. Res.
690 Lett., 16, 084061, 10.1088/1748-9326/ac16a3, 2021a.
- 691 Wang, Y., Fu, X., Wang, T., Ma, J., Gao, H., Wang, X., and Pu, W.: Large Contribution
692 of Nitrous Acid to Soil-Emitted Reactive Oxidized Nitrogen and Its Effect on Air
693 Quality, Environ. Sci. Technol., 57, 3516-3526, 10.1021/acs.est.2c07793, 2023b.



- 694 Wang, Y., Fu, X., Wu, D., Wang, M., Lu, K., Mu, Y., Liu, Z., Zhang, Y., and Wang, T.:
695 Agricultural Fertilization Aggravates Air Pollution by Stimulating Soil Nitrous
696 Acid Emissions at High Soil Moisture, *Environ. Sci. Technol.*, 55, 14556-14566,
697 10.1021/acs.est.1c04134, 2021b.
- 698 Wang, Y., Wang, J., Zhang, H., Janecek, N., Wang, Y., Zhou, M., Shen, P., Tan, J., He,
699 Q., Cheng, T., and Huang, C.: Impact of land use change on the urban-rural
700 temperature disparity in Eastern China, *Atmos. Environ.*, 308, 119850,
701 10.1016/j.atmosenv.2023.119850, 2023c.
- 702 Weber B, W. D., Tamm A, et al. : Biological soil crusts accelerate the nitrogen cycle
703 through large NO and HONO emissions in drylands, *Proc. Natl. Acad. Sci. U.S.A.*,
704 112(50): 15384-15389., 2015.
- 705 Wei, J., Li, Z., Li, K., Dickerson, R. R., Pinker, R. T., Wang, J., Liu, X., Sun, L., Xue,
706 W., and Cribb, M.: Full-coverage mapping and spatiotemporal variations of
707 ground-level ozone (O₃) pollution from 2013 to 2020 across China, *Remote Sens.*
708 *Environ.*, 270, 112775, 10.1016/j.rse.2021.112775, 2022.
- 709 Xu, W., Kuang, Y., Zhao, C., Tao, J., Zhao, G., Bian, Y., Yang, W., Yu, Y., Shen, C.,
710 Liang, L., Zhang, G., Lin, W., and Xu, X.: NH₃-promoted hydrolysis of NO₂
711 induces explosive growth in HONO, *Atmos. Chem. Phys.*, 19, 10557-10570,
712 10.5194/acp-19-10557-2019, 2019.
- 713 Yan, X., Ohara, T., and Akimoto, H.: Statistical modeling of global soil NO_x emissions,
714 *Global Biogeochem. Cycles*, 19, 10.1029/2004gb002276, 2005.
- 715 Ye, C., Gao, H., Zhang, N., and Zhou, X.: Photolysis of Nitric Acid and Nitrate on
716 Natural and Artificial Surfaces, *Environ. Sci. Technol.*, 50, 3530-3536,
717 10.1021/acs.est.5b05032, 2016.
- 718 Ye, C., Zhang, N., Gao, H., and Zhou, X.: Photolysis of Particulate Nitrate as a Source
719 of HONO and NO_x, *Environ. Sci. Technol.*, 51, 6849-6856,
720 10.1021/acs.est.7b00387, 2017.
- 721 Yue, X., Unger, N., Harper, K., Xia, X., Liao, H., Zhu, T., Xiao, J., Feng, Z., and Li, J.:
722 Ozone and haze pollution weakens net primary productivity in China, *Atmos.*
723 *Chem. Phys.*, 17, 6073-6089, 10.5194/acp-17-6073-2017, 2017.



- 724 Zaveri, R. A. and Peters, L. K.: A new lumped structure photochemical mechanism for
725 large-scale applications, *J. Geophys. Res.: Atmos.*, 104, 30387-30415,
726 10.1029/1999jd900876, 1999.
- 727 Zaveri, R. A., Easter, R. C., Fast, J. D., and Peters, L. K.: Model for Simulating Aerosol
728 Interactions and Chemistry (MOSAIC), *J. Geophys. Res.: Atmos.*, 113,
729 10.1029/2007jd008782, 2008.
- 730 Zhang, J., Ran, H., Guo, Y., Xue, C., Liu, X., Qu, Y., Sun, Y., Zhang, Q., Mu, Y., Chen,
731 Y., Wang, J., and An, J.: High crop yield losses induced by potential HONO
732 sources — A modelling study in the North China Plain, *Sci. Total Environ.*, 803,
733 149929, 10.1016/j.scitotenv.2021.149929, 2022a.
- 734 Zhang, J., Lian, C., Wang, W., Ge, M., Guo, Y., Ran, H., Zhang, Y., Zheng, F., Fan, X.,
735 Yan, C., Daellenbach, K. R., Liu, Y., Kulmala, M., and An, J.: Amplified role of
736 potential HONO sources in O₃ formation in North China Plain during autumn haze
737 aggravating processes, *Atmos. Chem. Phys.*, 22, 3275-3302, 10.5194/acp-22-
738 3275-2022, 2022b.
- 739 Zhang, L., Wang, T., Zhang, Q., Zheng, J., Xu, Z., and Lv, M.: Potential sources of
740 nitrous acid (HONO) and their impacts on ozone: A WRF-Chem study in a
741 polluted subtropical region, *J. Geophys. Res.: Atmos.*, 121, 3645-3662,
742 10.1002/2015jd024468, 2016.
- 743 Zhang, S., Sarwar, G., Xing, J., Chu, B., Xue, C., Sarav, A., Ding, D., Zheng, H., Mu,
744 Y., Duan, F., Ma, T., and He, H.: Improving the representation of HONO chemistry
745 in CMAQ and examining its impact on haze over China, *Atmos. Chem. Phys.*, 21,
746 15809-15826, 10.5194/acp-21-15809-2021, 2021.
- 747 Zhang, W., Tong, S., Jia, C., Wang, L., Liu, B., Tang, G., Ji, D., Hu, B., Liu, Z., Li, W.,
748 Wang, Z., Liu, Y., Wang, Y., and Ge, M.: Different HONO Sources for Three
749 Layers at the Urban Area of Beijing, *Environ. Sci. Technol.*, 54, 12870-12880,
750 10.1021/acs.est.0c02146, 2020.
- 751
752

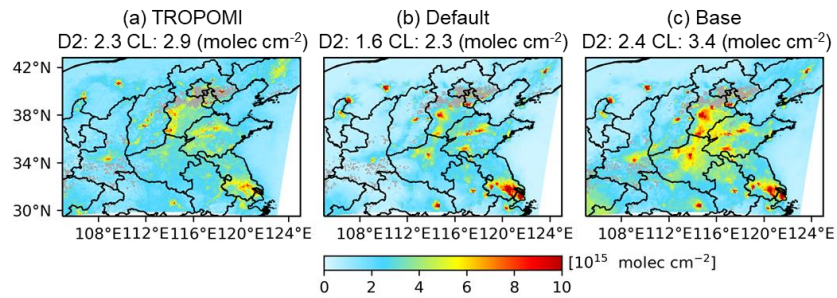


753

754 **Figure 1.** Distribution of the simulated monthly mean (a) soil NO_x emissions, (b) soil

755 HONO emissions, and (c) anthropogenic NO_x emissions in July 2018.

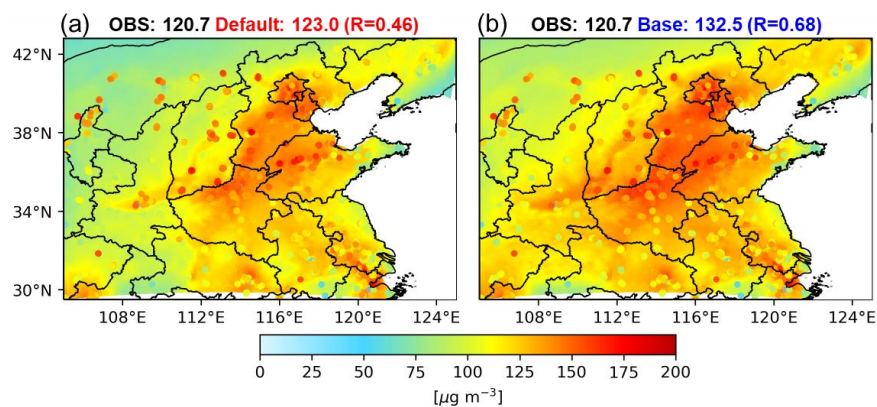
756



757

758 **Figure 2.** (a) Monthly mean tropospheric NO₂ VCD retrieved by TROPOMI measured
759 at 12:00–14:00 LT and simulated by (e) Default and (f) Base averaged over the same
760 periods in July 2018.

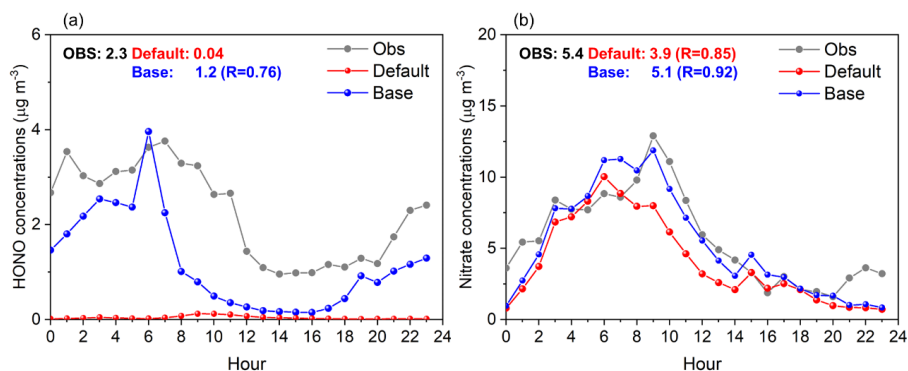
761



762

763 **Figure 3.** Distribution of observed (dots) and simulated (shaded) surface MDA8 O₃
764 from (a) Default and (b) Base in July 2018. Statistics in the upper corner of panels are
765 the monthly mean MDA8 O₃ concentrations averaged over the study region and the
766 spatial correlation coefficient R between observations and simulations.

767



768

769 **Figure 4.** Diurnal variation of observed (in grey) and simulated (Default in red and

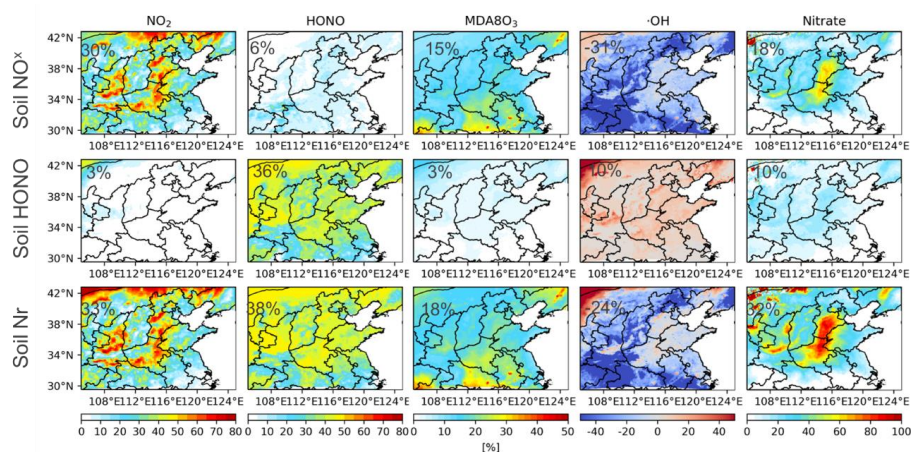
770 Base in blue) surface (a) HONO and (b) nitrate concentrations at a rural station in

771 Nanjing, with the mean value and temporal correlation coefficients (R) shown in the

772 upper right corner.

773

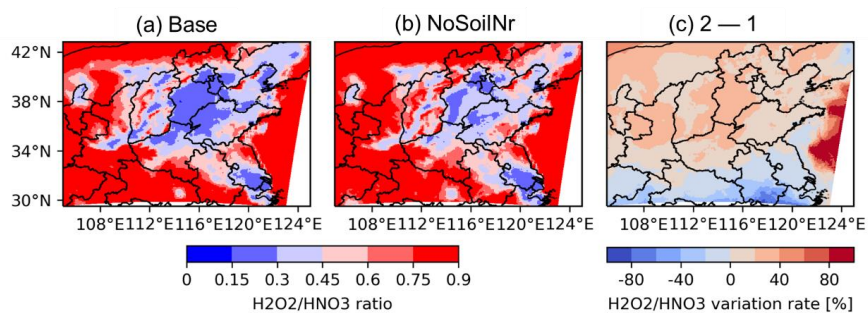
774



775

776 **Figure 5.** Simulated effects of soil Nr emissions on air quality. The first and second
777 rows show the contributions of soil NO_x and soil HONO emissions on monthly average
778 concentrations of NO₂, HONO, MDA8O₃, max-1h ·OH, and nitrate, respectively. The
779 third row shows the combined effect of soil Nr emissions on the species listed above.
780 Statistics in the upper right corner of each panel are the mean values averaged over the
781 study region.

782



783

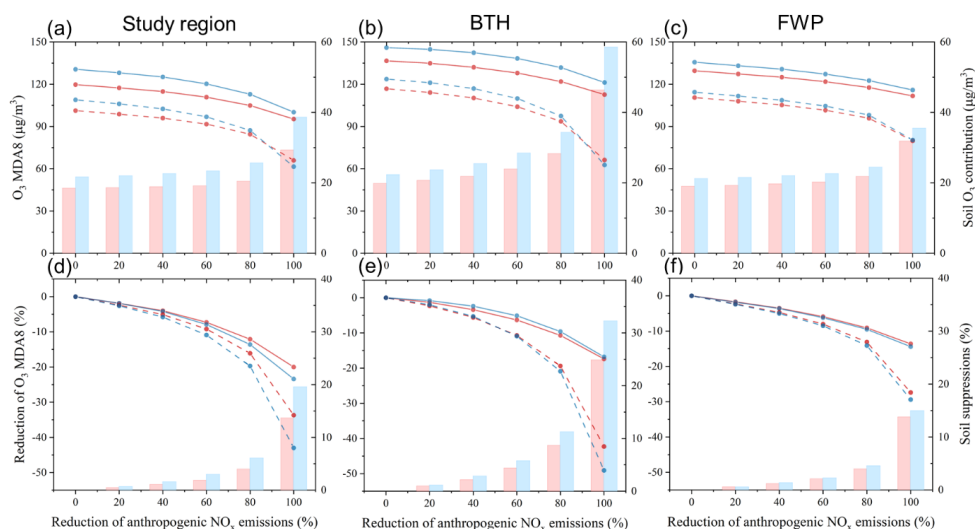
784 **Figure 6.** Distribution of the O₃ formation regimes (represented as H₂O₂/HNO₃ ratios)

785 for (a) Base simulation with the addition of soil Nr emissions and (b) NoSoilNr

786 simulation without the addition of soil Nr emissions. (c) Changes in the distribution of

787 O₃ formation regimes due to the soil Nr emissions

788



789

790 **Figure 7.** Role of soil Nr emissions in O₃ pollution regulation. The responses of MDA8

791 O₃ concentrations to the reductions of anthropogenic NO_x emissions (20%, 40%, 60%,

792 80% and 100%) relative to July 2018 levels, in the presence (solid line) and absence

793 (dotted line) of soil Nr emissions in the study region, BTH and FWP region. (The lines

794 in panels a-c and d-f are MDA8 O₃ concentrations and the relative reductions in MDA8

795 O₃ under different anthropogenic NO_x emission reductions, respectively. The red bars

796 (right y-axis) in panels a-c show the corresponding O₃ contribution from soil Nr

797 emissions, which is determined as the difference between the solid and dotted lines, and

798 the blue bars are the same as the red bars but for statistics in cropland. The red bars

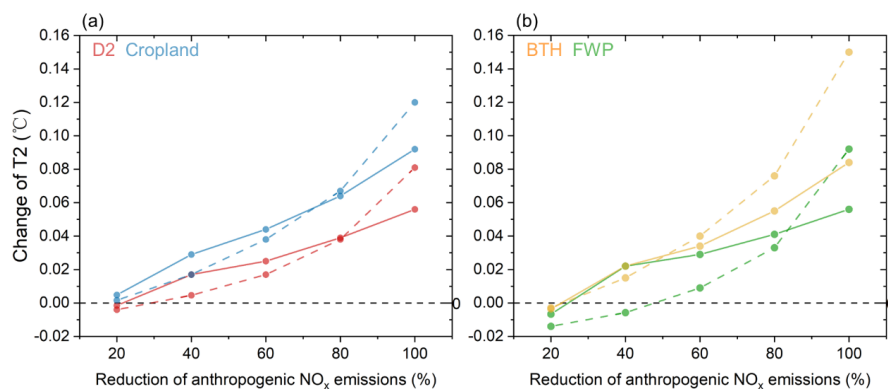
799 (right y-axis) in panels d-f show the suppression of O₃ pollution mitigated due to the

800 existence of soil Nr emissions, which are determined as the difference between the solid

801 and dotted lines, and the blue bars are the same as the red bars but for statistics in

802 cropland.)

803



804

805 **Figure 8.** The responses of air temperature at 2m (T2) to the reductions of
806 anthropogenic NO_x emissions (20%, 40%, 60%, 80% and 100%) relative to July 2018
807 levels in the presence (solid line) and absence (dotted line) of soil Nr emissions (a) in
808 the study region, (b) BTH and FWP region.

809